Liu *et al. Chem. Synth.* **2025**, *5*, 17
DOI: 10.20517/cs.2024.34

Chemical Synthesis

Research Article

Open Access

Decorating pore environment via cationic units of covalent organic frameworks for enhancing CO_2 reduction reaction

Minghao Liu[1,2], Guojuan Liu[1,3], Qing Xu[1,3,*], Gaofeng Zeng[1,3,*]

[1]CAS Key Laboratory of Low-Carbon Conversion Science and Engineering, Shanghai Advanced Research Institute (SARI), Chinese Academy of Sciences (CAS), Shanghai 201210, China.
[2]Department of Chemical and Environmental Engineering, University of Nottingham Ningbo China, Ningbo 315199, Zhejiang, China.
[3]University of Chinese Academy of Sciences, Beijing 100049, China.

[*]**Correspondence to:** Prof. Qing Xu, Prof. Gaofeng Zeng, CAS Key Laboratory of Low-Carbon Conversion Science and Engineering, Shanghai Advanced Research Institute (SARI), Chinese Academy of Sciences (CAS), 99 Haike Road, Shanghai 201210, China. E-mail: xuqing@sari.ac.cn; zenggf@sari.ac.cn

How to cite this article: Liu, M.; Liu, G.; Xu, Q.; Zeng, G. Decorating pore environment via cationic units of covalent organic frameworks for enhancing CO_2 reduction reaction. *Chem. Synth.* **2025**, *5*, 17. https://dx.doi.org/10.20517/cs.2024.34

Received: 9 Mar 2024 **First Decision:** 31 May 2024 **Revised:** 30 Jul 2024 **Accepted:** 7 Aug 2024 **Published:** 8 Jan 2025

Academic Editors: Guangshan Zhu, Jiangtao Jia, Wei Li **Copy Editor:** Dong-Li Li **Production Editor:** Dong-Li Li

Abstract

The conversion performance for electrocatalytic CO_2 reduction reaction (CO_2RR) relies on the affinity of CO_2 molecules. Ionic covalent organic frameworks (COFs) are promising platforms for CO_2RR due to the accessible catalytic sites in the skeleton, high CO_2 combination ability and the electronic conductivity. However, most ionic COFs are constructed via pre-functionalization of the monomers or post-modification of the skeleton, encountering incomplete loading or uneven distribution of the active sites. In this work, a cationic porphyrin-based COF using the (3-carboxypropyl)trimethylammonium and Co-porphyrin units is developed through the sub-stoichiometric bottom-up synthesis method to fine-tune the pore environment for modulating the binding ability of CO_2. Compared to base COFs, the cationic COFs exhibit improved electronic conductivity, high CO_2 adsorption uptakes and enhanced reducibility, further improving the electrocatalytic CO_2RR performance. Notably, the cationic COF achieves a high CO selectivity of 93% and a partial current density of 24.6 $mA{\cdot}cm^{-2}$. This work not only offers considerable insights for improving the catalytic performance of COFs through the cationic groups but also provides a stoichiometry method to modulate the pore environment.

Keywords: Covalent organic frameworks, CO_2 reduction reaction, modification strategy, cationic skeleton, CO_2 adsorption

INTRODUCTION

The electrocatalytic CO_2 reduction reaction (CO_2RR) is a crucial technology for reducing greenhouse gas concentrations and mitigating climate change[1-4]. Nowadays, the molecular catalysts, metallic nanoclusters and single atom catalysts (SACs) were employed to catalyse the CO_2RR[5-7]. However, the high energy barrier required to activate inert CO_2 and the weak binding interactions between CO_2 and catalysts impede catalytic activity and selectivity[8-10]. Consequently, it is imperative to enhance the interaction between CO_2 and reactants by modulating CO_2 adsorption behavior, which holds great significance for optimizing catalytic activity in CO_2RR.

Covalent organic frameworks (COFs), as emerging porous materials due to their high crystallinity, periodic channels, designable structures and robust stability, have attracted considerable attention for molecular adsorption, photo-/electro-catalysis, luminescent sensors and proton transport[11-20]. The porous materials including COFs and metal-organic frameworks (MOFs), constructed with catalytic building blocks, functional units and catalytic sites, have been employed as electrocatalysts towards oxygen reduction reaction (ORR) and oxygen evolution reaction (OER)[21-26]. In 2015, Lin *et al.* exhibited the porphyrin-COFs for CO_2RR using the heterophase strategy[27]. After that, the different dimensional topologies, functional groups, catalytic sites and linkages have been employed to improve the activity and selectivity towards CO_2 RR. For example, Han *et al.* reported three-dimensional COFs with abundant exposure active sites for CO_2 RR[28]. Furthermore, two dioxin-linked COFs were synthesized for improving CO_2RR activity through the tuneable electron transfer capacity[29]. However, these catalytic COFs mainly focused on the charge-neutral framework, lacking the exploration of ionic frameworks. The charge-neutral frameworks hinder the electron transferring to the catalytic sites, thus reducing the utilizing efficiency of catalytic sites. Ionic COFs as electrocatalysts possessed the enhanced electronic conductivity and improved electronic transport ability which can facilitate the intermediates transfer behavior. In addition, the abundant active sites promote the adsorption and activation of reactants in the CO_2RR[30].

In this work, we incorporated catalytic sites and cationic functional groups into 2D COFs for enhancing the CO_2RR selectivity and activity via the bottom-up synthesis method. The optimized COF [a cationic porphyrin-based COF using the (3-carboxypropyl)trimethylammonium (TMA-COF)] was built by adjusting stoichiometric ratios of the monomers using 4,4',4'',4'''-[1,4-phenylenebis(azanetriyl)]-tetrabenzaldehyde (PATA) unit as linkers, [5,10,15,20-tetrakis(4-aminophenyl)porphinato]-cobalt (CoTAPP) as catalytic sites and (3-carboxypropyl)trimethylammonium (TMA) as decorate units. Compared to Co-COF without TMA groups, the optimized COF exhibited higher selectivity and activity due to the enhanced CO_2 uptakes. Thus, this work provided not only a modification method for functionalizing COFs but also new insights for the energy conversion.

EXPERIMENTAL

The synthesis scheme and chemical structure of Co-COF and TMA-COF are shown in Scheme 1 and Supplementary Figures 1 and 2. More detailed information, including synthesis methods and materials, is presented in the Supplementary Materials.

RESULTS AND DISCUSSION

To identify the structure of two COFs, the Fourier transform infrared spectroscopy (FTIR) measurement was conducted. Specifically, the peaks at 1,620 cm^{-1} originated from C=N bonds of the as-synthesized COFs, suggesting the condensation of Schiff reactions [Supplementary Figure 3][31]. The ^{13}C nuclear magnetic resonance (NMR) also exhibited the structure of the prepared COFs. Specifically, the peaks at around 160 ppm were assigned to C=N bonds, suggesting the successful condensation of reactions for Co-COF and

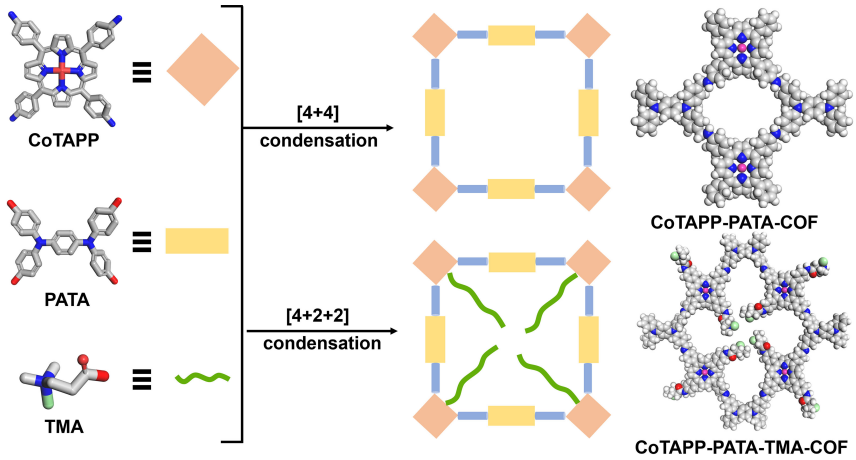

Scheme 1. Schematic diagram of Co-COF and TMA-COF using the Schiff condensation. COF: Covalent organic framework; TMA-COF: (3-carboxypropyl)trimethylammonium covalent organic framework.

TMA-COF [Supplementary Figure 4]. The peaks at around 56 and 65 ppm were contributed to the TMA units of TMA-COF [Supplementary Figure 4]. In addition, we used the inductively coupled plasma (ICP) and element analysis (EA) measurements to confirm that the contents of elements (C, N, O, H, Co) for Co-COF and TMA-COF. EA for the Co-COF: C, 77.06%; N, 10.98%; H, 4.48%; O, 4.89%. And EA for the Co-COF: C, 75.72%; N, 11.53%; H, 4.45%; O, 5.47%. In addition, the Co contents of Co-COF and TMA-COF were 2.72% and 2.43%, respectively. The crystalline structures of Co-COF and TMA-COF were explored and confirmed using the powder X-ray diffraction (PXRD) and "Materials Studio" software. Specifically, the PXRD patterns of the Co-COF illustrated the prominent peak at 5.56° with other peaks at 10.84° and 21.12° which were assigned to (011), (022) and (001) facets, respectively [Figure 1A]. Meanwhile, the simulated results and space group parameters suggested that the Co-COF adopted "PM" space groups and AA stacking models with the R_p = 2.38% and R_{wp} = 2.53% instead of AB stacking models [Figure 1B and Supplementary Figure 5].

In addition, the simulated PXRD patterns of the TMA-COF demonstrated the diffraction peaks at 5.61°, 9.55°, 10.84° and 20.84°, contributing to the (011), (202), (301) and (001) facets, respectively [Figure 1C]. Notably, the larger layer distance of (001) from TMA-COF than that of Co-COF manifested the electrostatic repulsion from the TMA groups. The Pawly refinement confirmed the AA stacking models of TMA-COF with the R_p = 2.53% and R_{wp} = 3.41% rather than AB stacking models [Figure 1D and Supplementary Figure 6].

The morphologies of obtained COFs were confirmed through the transmission electron microscopy (TEM) and field-emission scanning electron microscopy (FE-SEM). Specifically, the high-resolution TEM (HRTEM) images of Co-COF and TMA-COF illustrated that the dominant lattices with a d-space of 1.6 and 0.4 nm from (011) and (001) facet, respectively, further indicating the high crystallinity [Figure 1E and F]. In addition, the FE-SEM images showed that the Co-COF illustrated a bar shape that was composed of nanoparticles [Figure 1G]. The TMA-COF also exhibited a bar shape consisting of nanoparticles [Figure 1H]. Moreover, the energy dispersive X-ray spectroscopy (EDX) mappings confirmed the uniform distribution of these elements in COF fragments [Supplementary Figures 7 and 8]. Thermogravimetric analysis (TGA) manifested that the decompositions of Co-COF and TMA-COF reached only 8% and 11% at 550 °C, respectively [Supplementary Figure 9].

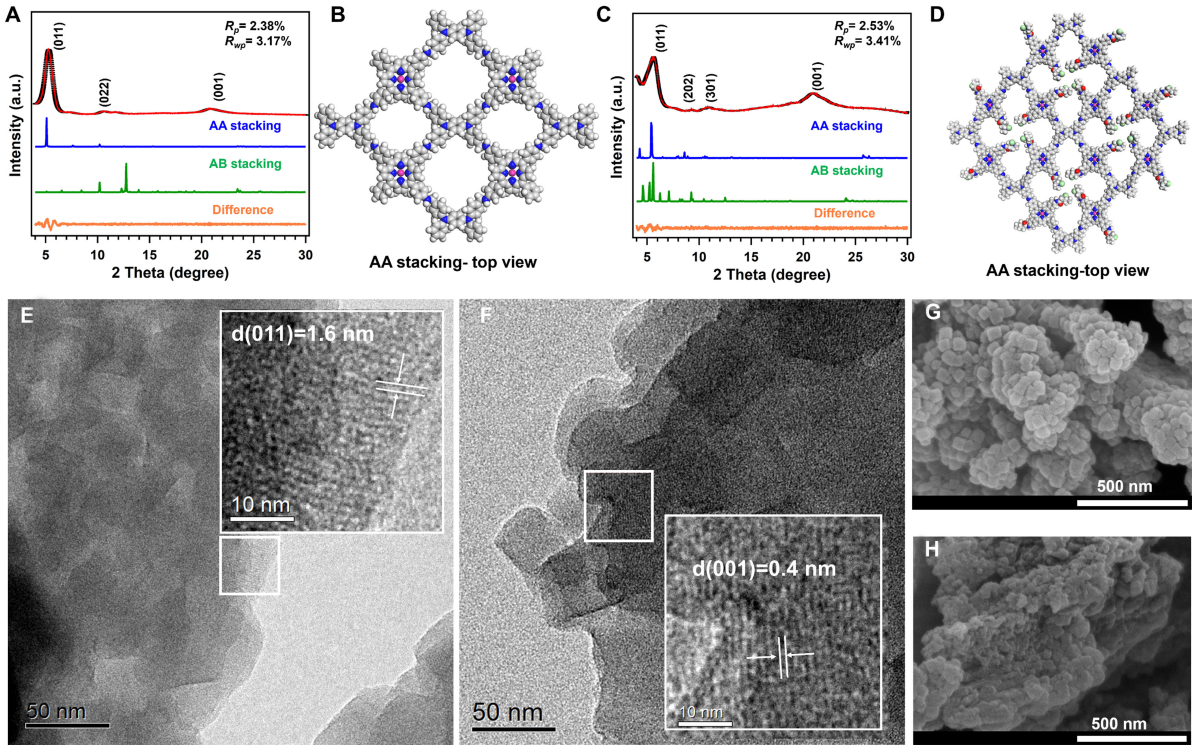

Figure 1. (A) The PXRD profile of the experimentally observed (black), Pawley refined (red), difference (orange), simulated using the AA (blue) and staggered AB (green) stacking modes; (B) Top view of theoretically modeled eclipsed-AA stacking model for the Co-COF (C-gray, N-blue, H-white, O-red, Co-pink); (C) The PXRD profile; (D) Top view of theoretically modeled eclipsed-AA stacking model for the TMA-COF; The TEM images of (E) Co-COF and (F) TMA-COF; The SEM images of (G) Co-COF and (H) TMA-COF. PXRD: Powder X-ray diffraction; COF: covalent organic framework; TMA-COF: (3-carboxypropyl)trimethylammonium covalent organic framework; TEM: transmission electron microscopy.

The inherent porosities of Co-COF and TMA-COF were analyzed by the N_2 sorption behavior. These two obtained COFs exhibited the type-I sorption curve, demonstrating microporous structures [Figure 2A]. The Brunner-Emmet-Teller specific surface areas of Co-COF and TMA-COF were 271.70 and 289.81 $m^2 \cdot g^{-1}$ with pore volumes of 0.38 and 0.47 $cm^3 \cdot g^{-1}$, respectively. Furthermore, the Co-COF and TMA-COF showed pore size distributions of 1.2 and 1.3 nm, respectively [Figure 2B and C]. Moreover, CO_2 adsorption isotherms were conducted to evaluate the CO_2 behavior of as-synthesized COFs. The TMA-COF illustrated the CO_2 uptakes of 21.33 $cm^3 \cdot g^{-1}$ at 298 K, respectively, which was higher than that of Co-COF (18.75 $cm^3 \cdot g^{-1}$, Figure 2D). These results indicated that introducing TMA units, which possessed strong CO_2 affinity capacity, was beneficial for the CO_2RR.

We adopted X-ray photoelectron spectroscopy (XPS) to study the atom and electron states. In particular, the XPS spectra showed peaks of all elements in orbitals (C, N, O and Co, Supplementary Figure 10). The high-resolution Co *2p* spectra of these two COFs displayed the peaks at ~781.38 eV assigned to the Co-N coordination from CoTAPP units [Figure 3A]. In addition, the N *1s* spectra of the Co-COF showed three peaks at 398.7, 399.8 and 401.5 eV, respectively, originating from iminic N, C=N, and C–N bonds[32-34]. Correspondingly, the N *1s* spectra of the TMA-COF demonstrated a new peak at ~402.1 eV attributed to the $C–N^+$ bonds from TMA groups [Figure 3B][33]. Moreover, we adopted the ultraviolet-visible (UV-Vis) spectroscopy to calculate band gaps [Supplementary Figure 11]. In detail, the Tauc plot illustrated the band gaps for Co-COF and TMA-COF were 1.91 and 1.73 eV, respectively, and the narrower bandgap for TMA-COF benefitted the electron transfer between intermediates and catalytic sites, further improving the

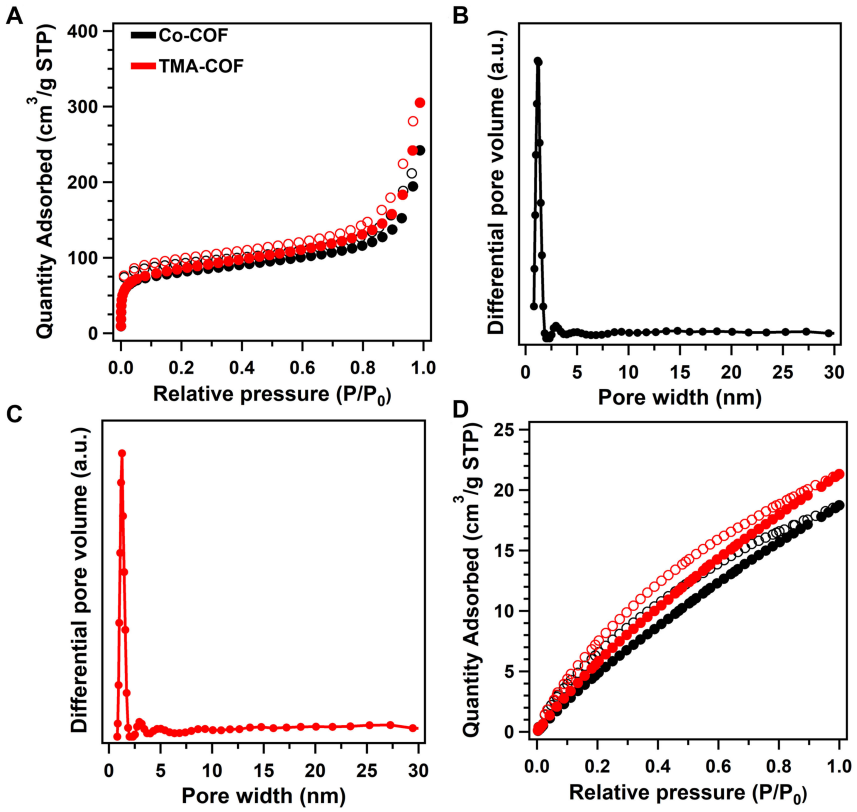

Figure 2. (A) The nitrogen-sorption isotherms at 77 K of Co-COF (black) and TMA-COF (red); The pore distribution curves of (B) Co-COF and (C) TMA-COF; (D) The CO_2 adsorption curves at 298 K for Co-COF (black) and TMA-COF (red). COF: Covalent organic framework; TMA-COF: (3-carboxypropyl)trimethylammonium covalent organic framework.

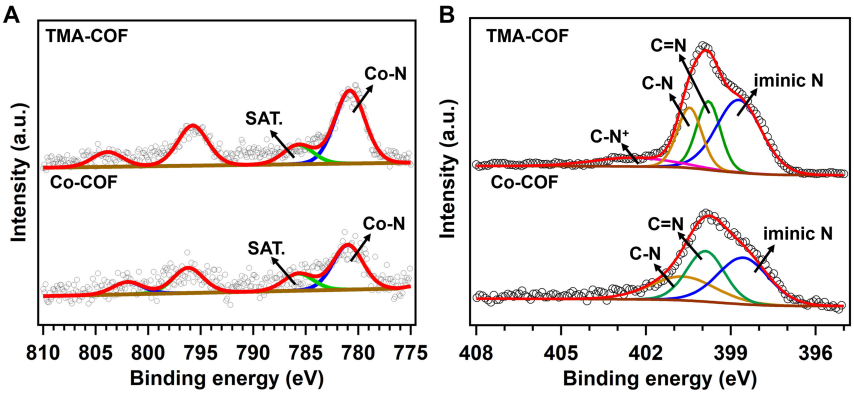

Figure 3. The XPS spectra of (A) Co *2p* and (B) N *1s* for Co-COF and TMA-COF. XPS: X-ray photoelectron spectroscopy; TMA-COF: (3-carboxypropyl)trimethylammonium covalent organic framework.

reaction kinetics [Supplementary Figure 12][35-36]. Mott-Schottky patterns showed that these two COFs belonged to n-type semiconductors based on the positive slope, indicating the potential for supplying electrons in electrocatalysis [Supplementary Figure 13][37]. Furthermore, the Nyquist plots of TMA-COF exhibited the charge transfer resistance (R_{ct}) value was 23 Ω, which was smaller than that of Co-COF (27 Ω), suggesting the TMA units can enhance the charge transfer capacity of COFs [Supplementary Figure 14].

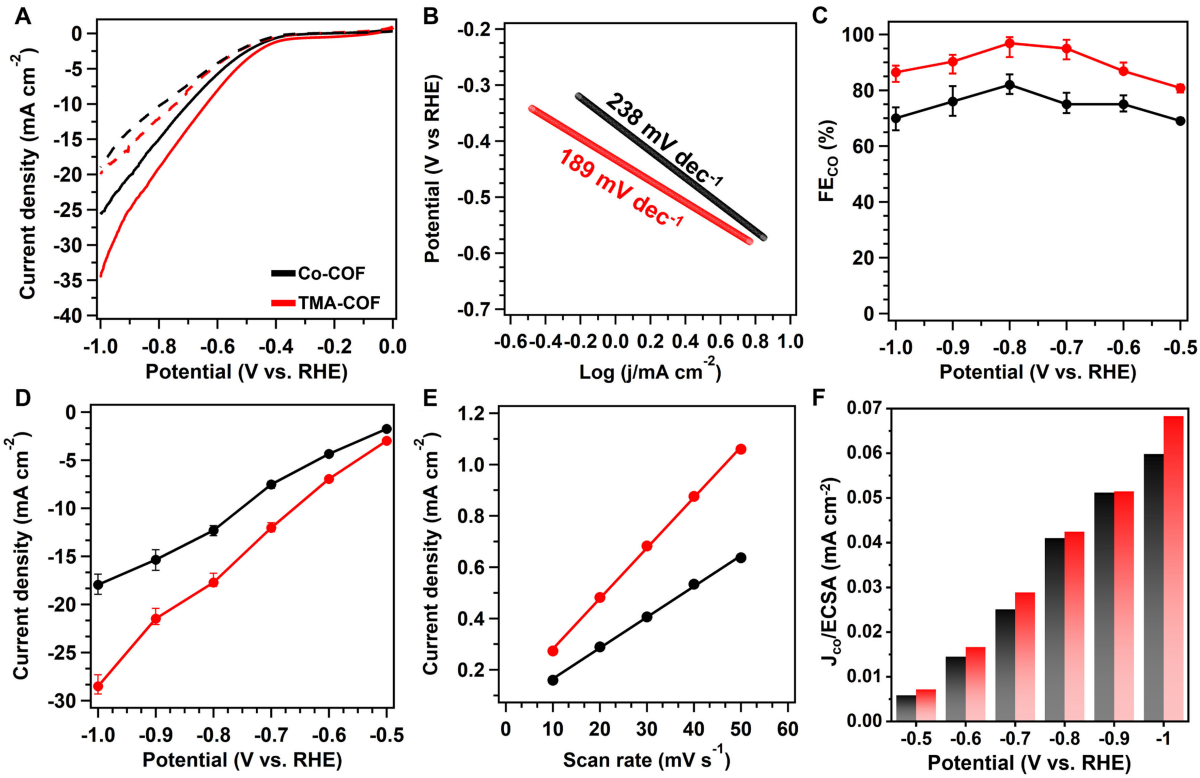

Figure 4. (A) LSV curves from -0.5 to -1.0 V in 0.5 M $KHCO_3$ under CO_2 atmosphere (line) and Ar atmosphere (dot); (B) Tafel slopes; (C) CO faradaic efficiency; (D) The partial CO current density; (E) The ECSA slopes; (F) The CO current density by the normalized ECSA for Co-COF (black) and TMA-COF (red). LSV: Linear sweep voltammetry; ECSA: electrochemically active surface area; COF: covalent organic framework; TMA-COF: (3-carboxypropyl)trimethylammonium covalent organic framework.

Considering these features of COFs, we evaluate the CO_2RR performance in 0.5 M $KHCO_3$ under CO_2 atmosphere within the applied potential range of -0.5 to -1.0 V *vs.* reversible hydrogen electrode (RHE). Specifically, the linear sweep voltammetry (LSV) curves suggested that the Co-COF and TMA-COF possessed higher current density in CO_2 atmosphere than in Ar atmosphere, revealing their efficient electrocatalytic CO_2RR activity [Figure 4A]. Meanwhile, the TMA-COF exhibited higher current density in the range of potentials than that of Co-COF, illustrating the high activity and electronic conductivity. Correspondingly, the Tafel slope of the Co-COF was 238 mV·dec^{-1}, which declined to 189 mV·dec^{-1} for TMA-COF, demonstrating the high kinetics [Figure 4B]. In addition, we used the gas and liquid chromatography to detect the products in the process of CO_2RR. The CO Faradaic efficiencies (FE_{CO}) of the Co-COF were 69%, 75%, 78%, 82%, 76%, and 70% with a floating value of ~4% from -0.5 to -1.0 V *vs.* RHE, respectively [Figure 4C and Supplementary Figure 15]. Additionally, the higher FE_{CO} values were observed on the TMA-COF with the increase of CO_2 uptakes. Specifically, it delivered FE_{CO} of 81%, 86%, 90%, 93%, 86% and 83% with a floating value of ~5%, in the same potential ranges, which are higher than that of other reported COF-based materials [Supplementary Figure 16 and Table 1]. Furthermore, the FE_{CO} of carbon nanotubes (CNTs) were below 0.22% from -0.5 to -1.0 V *vs.* RHE, respectively [Supplementary Figure 17]. In addition to the selectivity, we calculated the partial CO current density (j_{CO}) to investigate the activity of two COFs. The Co-COF and TMA-COF exhibited the highest j_{CO} of 17.9 and 28.5 mA·cm^{-2} at -1.0 V *vs.* RHE [Figure 4D]. To confirm the internal catalytic activity, the turnover frequency (TOF) was calculated [Supplementary Figure 18]. TMA-COF demonstrated a TOF value of 1,171 h^{-1}, higher than that of Co-COF (538 h^{-1}) at -1.0 V. These results manifested that the catalytic activity and selectivity would be improved with

the enhanced combination between CO_2 and reactants.

The electrochemical double layer capacitances (C_{dl}) investigated the catalytic density of active sites through the cyclic voltammetry (CV) measurement [Supplementary Figure 19]. The C_{dl} values for the Co-COF and TMA-COF were 12.0 and 16.7 mF·cm^{-2}, respectively, indicating the TMA-COF possessed more exposure active sites than Co-COF [Figure 4E]. Furthermore, the electrochemically active surface areas (ECSAs) of obtained COFs were calculated by the ratio of C_{dl} and C_s, in which the C_s is 0.04 mF cm^{-2}[38]. We normalized CO current densities using j_{CO} per ECSA. Specifically, TMA-COF exhibited higher $j_{CO/ECSA}$ in the range of -0.5 to -1.0 V *vs.* RHE, suggesting the improvement of the electrochemical activity through the ionic groups [Figure 4F].

The stability of TMA-COF was measured in 0.5 M $KHCO_3$. The activity for CO_2RR was well preserved for 30 h [Supplementary Figure 20]. The FE_{CO} and the value of j/j_0 were over 90%. In addition, the PXRD profiles confirmed the maintained crystallinity [Supplementary Figure 21]. Meanwhile, the XPS spectra of Co *2p* and N *1s* also proved that the atomic states maintained the coordination after the stability measurement, confirming the reliable stability [Supplementary Figures 22 and 23][39].

CONCLUSIONS

In summary, a catalytic COF with cationic functional groups was developed using the sub-stoichiometric bottom-up synthesis method. The experiments suggested that the combination of catalytic sites and cationic groups can modulate the band structure and CO_2 adsorption behavior. This cationic COF illustrated the high CO_2RR performance with FE_{CO} of 93% at -0.8 V *vs.* RHE. Thus, constructing ionic structures which can modulate the interaction with guests and regulate the location of charge groups is a prospective way for understanding the catalytic mechanisms, further providing new insights for the energy conversion.

DECLARATIONS

Acknowledgments

Authors acknowledged the support from the PhD thesis from the University of Nottingham Ningbo China.

Authors' contributions

Made substantial contributions to conception and design of the study and performed data analysis and interpretation: Liu M, Liu G, Xu Q, Zeng G

Performed data acquisition and provided administrative, technical, and material support: Liu M, Liu G, Xu Q, Zeng G

Availability of data and materials

The raw data supporting the findings of this study are available within this Article and its Supplementary Materials. Further data is available from the corresponding authors upon request.

Financial support and sponsorship

The National Natural Science Foundation of China (52303288, 22075309, 22378413), Science and Technology Innovation Plan of the Science and Technology Commission of Shanghai Municipality (22ZR1470100, 23DZ1202600, 23DZ1201804), the Youth Innovation Promotion Association of Chinese Academy of Sciences (E324441401), Sichuan Province Engineering Technology Research Center of Novel CN Polymeric Materials (CNP-C-240201), and Biomaterials and Regenerative Medicine Institute Cooperative Research Project Shanghai Jiao Tong University School of Medicine (2022LHA09).

Conflicts of interest

All authors declared that there are no conflicts of interest.

Ethical approval and consent to participate

Not applicable.

Consent for publication

Not applicable.

Copyright

REFERENCES

1. Chen, Q.; Wang, X.; Zhou, Y.; et al. Electrocatalytic CO_2 reduction to C_{2+} products in flow cells. *Adv. Mater.* **2024**, *36*, e2303902. DOI PubMed
2. Lai, W.; Qiao, Y.; Zhang, J.; Lin, Z.; Huang, H. Design strategies for markedly enhancing energy efficiency in the electrocatalytic CO_2 reduction reaction. *Energy. Environ. Sci.* **2022**, *15*, 3603-29. DOI
3. Li, X.; Yu, J.; Jaroniec, M.; Chen, X. Cocatalysts for selective photoreduction of CO_2 into solar fuels. *Chem. Rev.* **2019**, *119*, 3962-4179. DOI PubMed
4. Lu, M.; Zhang, M.; Liu, J.; et al. Covalent organic framework based functional materials: important catalysts for efficient CO_2 utilization. *Angew. Chem. Int. Ed. Engl.* **2022**, *61*, e202200003. DOI PubMed
5. Ma, W.; He, X.; Wang, W.; Xie, S.; Zhang, Q.; Wang, Y. Electrocatalytic reduction of CO_2 and CO to multi-carbon compounds over Cu-based catalysts. *Chem. Soc. Rev.* **2021**, *50*, 12897-914. DOI
6. Xiao, C.; Zhang, J. Architectural design for enhanced C_2 product selectivity in electrochemical CO_2 reduction using Cu-based catalysts: a review. *ACS. Nano.* **2021**, *15*, 7975-8000. DOI PubMed
7. Xie, C.; Niu, Z.; Kim, D.; Li, M.; Yang, P. Surface and interface control in nanoparticle catalysis. *Chem. Rev.* **2020**, *120*, 1184-249. DOI PubMed
8. Yang, P. P.; Gao, M. R. Enrichment of reactants and intermediates for electrocatalytic CO_2 reduction. *Chem. Soc. Rev.* **2023**, *52*, 4343-80. DOI PubMed
9. Zhang, X.; Zhang, Z.; Li, H.; et al. Insight into heterogeneous electrocatalyst design understanding for the reduction of carbon dioxide. *Adv. Energy. Mater.* **2022**, *12*, 2201461. DOI
10. Zhang, Z.; Huang, X.; Chen, Z.; et al. Membrane electrode assembly for electrocatalytic CO_2 reduction: principle and application. *Angew. Chem. Int. Ed. Engl.* **2023**, *62*, e202302789. DOI PubMed
11. Guo, L.; Yang, L.; Li, M.; Kuang, L.; Song, Y.; Wang, L. Covalent organic frameworks for fluorescent sensing: recent developments and future challenges. *Coord. Chem. Rev.* **2021**, *440*, 213957. DOI
12. Haug, W. K.; Moscarello, E. M.; Wolfson, E. R.; McGrier, P. L. The luminescent and photophysical properties of covalent organic frameworks. *Chem. Soc. Rev.* **2020**, *49*, 839-64. DOI PubMed
13. Jin, E.; Asada, M.; Xu, Q.; et al. Two-dimensional sp^2 carbon-conjugated covalent organic frameworks. *Science* **2017**, *357*, 673-6. DOI PubMed
14. Li, Z.; Sheng, L.; Wang, H.; et al. Three-dimensional covalent organic framework with ceq topology. *J. Am. Chem. Soc.* **2021**, *143*, 92-6. DOI PubMed
15. Weng, W.; Guo, J. Chiral covalent organic framework films with enhanced photoelectrical performances. *J. Am. Chem. Soc.* **2024**, *146*, 13201-9. DOI PubMed
16. Liu, L.; Gong, Y.; Tong, Y.; et al. Imidazole-linked fully conjugated covalent organic framework for high-performance sodium-ion battery. *CCS. Chem.* **2024**, *6*, 1255-63. DOI
17. Sun, C.; Sheng, D.; Wang, B.; Feng, X. Covalent organic frameworks for extracting water from air. *Angew. Chem. Int. Ed. Engl.* **2023**, *62*, e202303378. DOI
18. Xu, X.; Wu, X.; Xu, K.; Xu, H.; Chen, H.; Huang, N. Pore partition in two-dimensional covalent organic frameworks. *Nat. Commun.* **2023**, *14*, 3360. DOI PubMed PMC
19. Yaghi, O. M. Reticular chemistry in all dimensions. *ACS. Cent. Sci.* **2019**, *5*, 1295-300. DOI PubMed PMC
20. Zhou, T.; Wang, L.; Huang, X.; et al. PEG-stabilized coaxial stacking of two-dimensional covalent organic frameworks for enhanced photocatalytic hydrogen evolution. *Nat. Commun.* **2021**, *12*, 3934. DOI PubMed PMC
21. Li, Z.; Deng, T.; Ma, S.; et al. Three-component donor-π-acceptor covalent-organic frameworks for boosting photocatalytic hydrogen evolution. *J. Am. Chem. Soc.2023*, 8364-74. DOI PubMed
22. Lin, Z.; Liu, S.; Weng, W.; Wang, C.; Guo, J. Photostimulated covalent linkage transformation isomerizing covalent organic frameworks for improved photocatalytic performances. *Small* **2024**, *20*, e2307138. DOI PubMed

23. Liu, M.; Fu, Y.; Bi, S.; et al. Dimensionally-controlled interlayer spaces of covalent organic frameworks for the oxygen evolution reaction. *Chem. Eng. J.* **2024**, *479*, 147682. DOI
24. Zhang, Y.; Zhang, X.; Jiao, L.; Meng, Z.; Jiang, H. L. Conductive covalent organic frameworks of polymetallophthalocyanines as a tunable platform for electrocatalysis. *J. Am. Chem. Soc.* **2023**, *145*, 24230-9. DOI PubMed
25. Zhu, H. J.; Lu, M.; Wang, Y. R.; et al. Efficient electron transmission in covalent organic framework nanosheets for highly active electrocatalytic carbon dioxide reduction. *Nat. Commun.* **2020**, *11*, 497. DOI PubMed PMC
26. Pan, Y.; Li, Y.; Nairan, A.; et al. Constructing FeNiPt@C trifunctional catalyst by high spin-induced water oxidation activity for Zn-Air battery and anion exchange membrane water electrolyzer. *Adv. Sci.* **2024**, *11*, e2308205. DOI PubMed PMC
27. Lin, S.; Diercks, C. S.; Zhang, Y. B.; et al. Covalent organic frameworks comprising cobalt porphyrins for catalytic CO_2 reduction in water. *Science* **2015**, *349*, 1208-13. DOI PubMed
28. Han, B.; Jin, Y.; Chen, B.; et al. Maximizing electroactive sites in a three-dimensional covalent organic framework for significantly improved carbon dioxide reduction electrocatalysis. *Angew. Chem. Int. Ed. Engl.* **2022**, *61*, e202114244. DOI PubMed
29. Yue, Y.; Cai, P.; Xu, K.; et al. Stable bimetallic polyphthalocyanine covalent organic frameworks as superior electrocatalysts. *J. Am. Chem. Soc.* **2021**, *143*, 18052-60. DOI PubMed
30. Liu, M.; Xu, Q.; Zeng, G. Ionic covalent organic frameworks in adsorption and catalysis. *Angew. Chem. Int. Ed. Engl.* **2024**, *63*, e202404886. DOI PubMed
31. Zhang, Q.; Dong, S.; Shao, P.; et al. Covalent organic framework-based porous ionomers for high-performance fuel cells. *Science* **2022**, *378*, 181-6. DOI PubMed
32. Zhang, M.; Liao, J. P.; Li, R. H.; et al. Green synthesis of bifunctional phthalocyanine-porphyrin cofs in water for efficient electrocatalytic CO_2 reduction coupled with methanol oxidation. *Natl. Sci. Rev.* **2023**, *10*, nwad226. DOI PubMed PMC
33. Song, Y.; Zhang, J. J.; Dou, Y.; et al. Atomically thin, ionic-covalent organic nanosheets for stable, high-performance carbon dioxide electroreduction. *Adv. Mater.* **2022**, *34*, e2110496. DOI PubMed
34. Baker, C. B. D.; Enache, M.; Küster, K.; et al. Structural transformation of surface-confined porphyrin networks by addition of Co atoms. *Chemistry* **2021**, *27*, 12430-6. DOI PubMed PMC
35. Yao, N.; Wang, G.; Jia, H.; et al. Intermolecular energy gap-induced formation of high-valent cobalt species in CoOOH surface layer on cobalt sulfides for efficient water oxidation. *Angew. Chem. Int. Ed. Engl.* **2022**, *61*, e202117178. DOI PubMed
36. Yang, D.; Yu, H.; He, T.; et al. Visible-light-switched electron transfer over single porphyrin-metal atom center for highly selective electroreduction of carbon dioxide. *Nat. Commun.* **2019**, *10*, 3844. DOI PubMed PMC
37. Huang, Q.; Niu, Q.; Li, X. F.; et al. Demystifying the roles of single metal site and cluster in CO_2 reduction via light and electric dual-responsive polyoxometalate-based metal-organic frameworks. *Sci. Adv.* **2022**, *8*, eadd5598. DOI PubMed PMC
38. Li, N.; Si, D. H.; Wu, Q. J.; Wu, Q.; Huang, Y. B.; Cao, R. Boosting electrocatalytic CO_2 reduction with conjugated bimetallic Co/Zn polyphthalocyanine frameworks. *CCS. Chem.* **2023**, *5*, 1130-43. DOI
39. Liu, M. Rational design of functional covalent organic frameworks for the oxygen and Carbon Dioxide reduction reactions. PhD thesis, University of Nottingham Ningbo China (UNNC), 2024. Available from: https://research.nottingham.edu.cn/en/studentTheses/rational-design-of-functional-covalent-organic-frameworks-for-the. [Last accessed on 9 Aug 2024]

Minghao Liu

Minghao Liu received his Ph.D. in 2024 from the joint program of Shanghai Advanced Research Institute (SARI) and University of Nottingham Ningbo China (UNNC). His current research interests focus on the synthesis of crystalline porous materials (MOF- and COF-based composites) and their applications in energy conversion and ion confinement.

Dr. Guojuan Liu

Dr. Guojuan Liu received her M.S. degree from Tianjin University in 2014 before joining Shanghai Advanced Research Institute (SARI), Chinese Academy of Sciences (CAS), where she obtained her Ph.D. in 2024. Currently, she works as an engineer at SARI. Her research interests focus on energy conversion and porous materials designs.

Prof. Qing Xu

Prof. Qing Xu received his M.S. degree in 2015 from Shanghai Jiao Tong University and his Ph.D. in 2018 from the Institute of Molecular Science (IMS), The Graduate University for Advanced Studies (SOKENDAI). He is an associate professor at Shanghai Advanced Research Institute, Chinese Academy of Sciences (CAS). His research interests focus on the synthesis and functionalization of covalent organic frameworks.

Prof. Gaofeng Zeng

Prof. Gaofeng Zeng received his B.E. degree from Dalian University of Technology (DUT) in 2002 and his Ph.D. from the Dalian Institute of Chemical Physics, Chinese Academy of Sciences (DICP) in 2009. Before joining Shanghai Advanced Research Institute, Chinese Academy of Sciences (SARI), he worked as a postdoctoral fellow at King Abdullah University of Science and Technology (KAUST) from 2009 to 2012. He is currently a professor and group leader at SARI, where his research centers on separation processes and energy conversion on nano-porous designs.